Appl. Phys. A (2015) 118:125–129
DOI 10.1007/s00339-014-8808-2

Applied Physics A
Materials Science & Processing

Ablation of metal thin films using femtosecond laser Bessel vortex beams

Ramazan Sahin · Tansu Ersoy · Selcuk Akturk

Received: 13 June 2014 / Accepted: 29 September 2014 / Published online: 9 October 2014

Abstract Femtosecond lasers can provide submicron ablation resolution, making them suitable and attractive for various micro/nanofabrication applications. Laser beam shaping lends further advantages and increases the versatility of these sources. In this work, we report on the use of femtosecond laser pulses with first-order Bessel function (Bessel vortex) beam profiles in ablation of metal thin films. The diffraction-free nature of Bessel beams provides significant convenience regarding alignment and repeatability. Ablation profiles with Bessel vortex beams generally consist of single or multiple concentric rings, determined by pulse fluence on target. We investigate single-pulse ablation behavior with two laser wavelengths (1,030 and 515 nm) and three different Bessel beam cone angles. For each case, we measure inner and outer ring diameters and compare our results with theoretical calculations.

1 Introduction

Ultrafast lasers with femtosecond (fs) pulse durations have been widely used for material processing applications at micrometer [1] and nanometer scale [2]. With these laser sources, thermal effects are minimized, and high-quality structures are routinely generated. The nonlinear optical and deterministic nature of ablation process also allows to reach sub-wavelength feature resolutions, by keeping the pulse fluence near ablation threshold [3, 4]. In these processes, Gaussian laser beams are commonly focused tightly by high numerical aperture (NA) objective lenses. The resulting short depth of focus and strong divergence requires critical sample positioning and angular alignment. On the other hand, it was recently shown that non-diffracting Bessel beams can provide significant advantages in fs laser material processing [5, 6]. Bessel beams have focal depths much larger as compared to Gaussian beams of the same spot sizes [7], and their transverse widths stay unchanged within this depth. As a result, sample alignment is much less critical with Bessel beams. In addition, high NA and short-wavelength Bessel beams are easy to generate with negligible optical aberrations, simply by using proper conical lenses (axicons). With these virtues, Bessel beams are used for processing of nanometer structures in transparent materials [8], metal thin films [9] and graphene [10, 11].

Optical vortices are another special beam classes, also used in laser material processing. In general, these beams possess a phase singularity, hence zero-intensity zone at their centers [12]. Wavefronts around phase singularities take helical form, and the rotation of helical wavefront is described by topological charge (m). After the beam propagates distance of $m \times \lambda$ (λ is wavelength of light beam), helical wavefronts repeat themselves. In addition, optical vortex photons also carry angular momentum, quantized by $m \times \hbar$. Optical vortices can be produced by various methods such as computer-generated holograms [13], using cylindrical lenses [14] or spiral phase plates (SPP) [15, 16].

These interesting physical properties and ring-like shapes of vortex beams can also be exploited for laser applications. For example, their angular momentum can be transferred to laser-trapped particles and induce rotations [17]. Regarding material processing, Hnatovsky et al. [18] investigated $m = +2$ vortex beam ablation of fused silica

R. Sahin (✉) · T. Ersoy · S. Akturk
Department of Physics Engineering, Istanbul Technical University, Maslak 34469, Istanbul, Turkey
e-mail: rsahin@itu.edu.tr

and soda lime glass and demonstrated micrometer-size rings with <100-nm groove thickness. Same research group also studied ablation of Si crystal by means of circularly polarized vortex beams with topological charge $m = 1$ and found out that right or left handed of polarization affects the ablation shape [19]. In a very recent study, graphene was ablated to microdisk and nanodisk shapes using Bessel vortex beams with different topological charges [11].

In this work, we exploit the advantages of non-diffracting Bessel beams together with properties of optical vortices to generate ring-like structure in metal (gold) thin films. We present a detailed study of Bessel vortex ablation behavior, using different laser wavelengths and axicon angles. As opposed to doughnut-shaped Laguerre–Gaussian vortex beams, Bessel vortices posses large number of concentric rings. As a result, their ablation profiles may yield single or multiple rings, depending on the pulse fluence. In all cases, at the center of the ablation zone (corresponding to zero intensity), a disk-like particle is left. The diameter of this disk decreases with increasing the pulse fluence. In our experiments, we observed diameters as small as 200 nm. Detailed analysis of ablation sizes is shown below. Our results show that Bessel vortex beam ablation on metal thin films can provide significant convenience for micrometer or nanometer scale fabrication of special structures such as isolated rings, concentric rings and isolated nanoparticles.

2 Beam shaping and ablation experiments

Gaussian laser beams can be turned into Bessel beams simply by passing them through an axicon. In this way, a typical TEM_{00} Gaussian beam yields zeroth-order Bessel beam. To generate Bessel vortex beams, one can either pass higher-order (mth-order TEM_{0m}) Laguerre–Gaussian beam through an axicon [20], or use TEM_{00} profile by adding a SPP of topological charge m. In both cases, the resulting Bessel vortex beam has a transverse profile closely approximated by

$$I(r) = J_m^2(k_r r) \tag{1}$$

where r is the radial coordinate, J_m is the mth-order Bessel function of the first kind and k_r is the transverse wavevector. The k_r in Eq. 1 is given by

$$k_r = \frac{2\pi}{\lambda}\sin\beta \tag{2}$$

where β is exit beam half cone angle after the axicon and given by $\beta = \alpha \sin(n \sin\alpha) - \alpha$, λ is the incident laser wavelength, n is the refractive index and α is the base angle of the axicon.

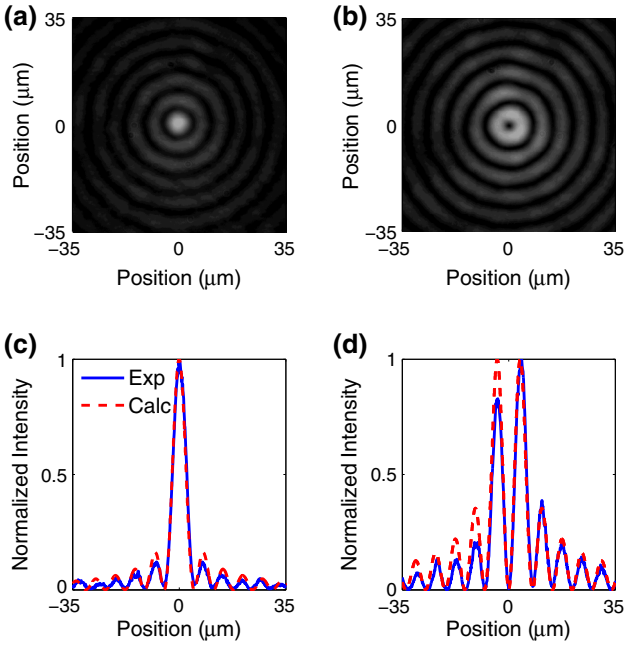

Fig. 1 CCD camera images of **a** zeroth-order and **b** first-order (vortex) Bessel beams. Data are taken with 1,030 nm wavelength and $\alpha = 10°$ base angle axicon. For clarity of outer rings, square root of the intensity data is taken. **c**, **d** shows cross sections from centers of these beams, compared to theoretical calculations

Except for the zeroth order (which has a central peak), intensity profiles of these Bessel beams comprise of concentric rings with different diameters (see Fig. 1). Intensity of innermost ring is maximum, and its diameter increases with m.

In the experiments, we use a Yb:Glass fs laser system (Amplitude Systemes, s-pulse) that produces 550 fs pulses with a central wavelength of 1,030 nm. The laser output is very nearly Gaussian (TEM_{00}). To generate Bessel beams and vortices, we use spiral phase plate of topological charge $m = 1$, and axicons with different base angles. We detect the beam profiles using a CCD camera, after magnification by a microscope objective. Figure 1 shows some typical measured beam profiles (for zeroth- and first-order Bessel beams) and their cross sections. The intensity profiles closely match calculated Bessel functions of corresponding order.

After the beam shaping steps, we perform ablation studies. The ablation setup is sketched in Fig. 2. By using external triggering, we operate the laser in single-pulse (at a given point on target) mode. Average power is controlled by a half waveplate and a polarizer. We also generate second harmonic of the laser (at 515 nm) using a BBO crystal. Ablation experiments are done with two wavelengths (1,030 and 515 nm) and three different axicon base angles (10°, 25° and 40°). Sample is placed on a computer-controlled, three-dimensional piezo translation stage (Mad City Labs, Nano3D 200).

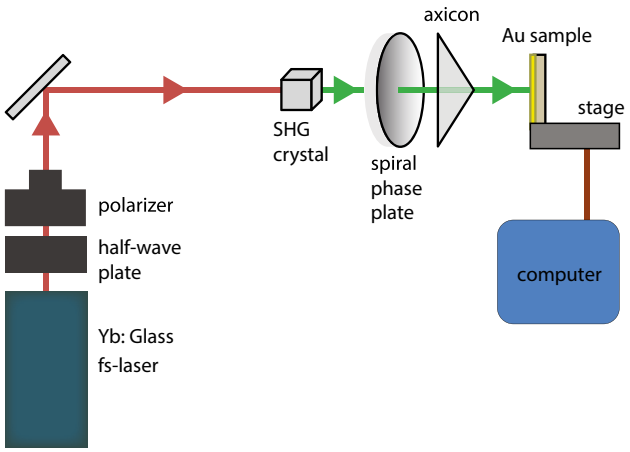

Fig. 2 Experimental setup used for Bessel vortex ablation process

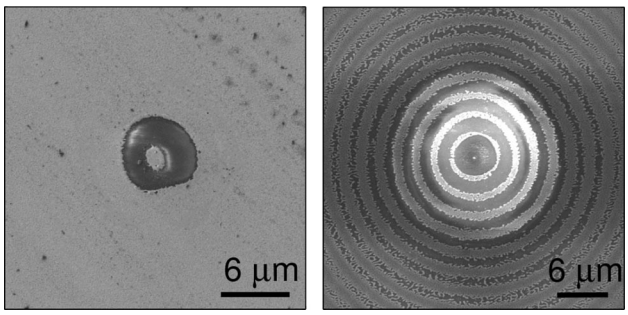

Fig. 3 SEM images of single and multiple ring ablation profiles. *Light-colored* regions are Au, *dark regions* are glass substrate. In single-ring case 515 nm wavelength and 10° axicon, in multi-ring case 1,030 nm wavelength and 25° axicon were used

Table 1 Calculated diameters of central rings of Bessel vortices for the wavelengths and axicon angles used in the experiments

λ/α (nm)	10° (μm)	25° (μm)	40° (μm)
1,030	7.53	2.72	1.26
515	3.69	1.33	0.60

As ablation samples, we use Au/Cr thin films on quartz. The films are coated using thermal evaporation technique under 10^{-7} mbar pressure. The Au/Cr film is fabricated as a 25-nm Au film with a 5-nm Cr sub-layer (to ensure adhesion of Au to substrate). Substrate is heated at 300 °C during the process to decrease surface roughness. Evaporation rate is kept constant at 0.05 nm/s, and sample is rotated for better uniformity. After ablation experiments, samples are imaged under an optical metallurgical microscope and scanning electron microscope (SEM).

3 Results and discussion

The ablation profiles on Au films, generated by Bessel vortices, are determined by pulse fluence on target. Due to the deterministic nature of fs laser ablation, regions of sample that are exposed to fluences above ablation threshold are evaporated, while the other regions remain almost intact. As a result, as can be interpreted from Fig. 1, depending on the fluence relative to ablation threshold, one can obtain single or multiple ring structures. Typical profiles for both cases are shown in Fig. 3.

As mentioned above, in our experiments, we use 1,030 and 515 nm wavelengths and three different axicons. The dimensions of rings are determined by both λ and α. Table 1 shows calculated diameters (distance between first peaks) of central rings of Bessel vortices (J_1) for our experimental parameters. When the fluence exceeds the ablation threshold and as it increases, inner/outer diameters of the central ablated rings become smaller/bigger than the values on Table 1.

For each of the wavelengths and axicon angles mentioned above, we perform single-shot ablation experiments on samples. We start near ablation threshold and gradually increase the pulse energy. As the energy increases, the central disk-like structure gets smaller and number of rings observed on the Au film increases.

In order to quantify ablation dimensions, we concentrate on the innermost ring (and the central disk), which are present in all cases (above threshold). We increase pulse energy until the central disk becomes completely invisible under microscope. For each ablation spot, we measure inner and outer diameters of the innermost ring. The results are presented in Fig. 4. For the case of 515 nm and 40°, ring pattern became irregular and meaningful measurements could not be taken, for reasons discussed below.

We also calculate expected ring dimensions (shown as solid lines in Fig. 4) by using theoretical Bessel vortex profiles together with experimental thresholds. Positions at which the calculated fluence equals the threshold yield ablation boundaries. Due to the weak electron–phonon coupling in Au [21], central disks formed by Bessel vortex ablation are also affected by melting dynamics and corresponding surface tensions. Melting and re-solidification for high pulse energy regimes cause hemispherical-like structures, noticeable in Fig. 5. These mechanisms also result in deviations from theoretical diameter calculations shown in Fig. 4.

Based on our results, the Bessel vortex ablation behavior can be summarized as follows. When the pulse energy is within approximately 3 times the ablation threshold, only the first Bessel lobe causes ablation and single-ring structures are obtained on the sample surface. At the center, a disk-like particle is left (see Fig. 5, left part). This isolated

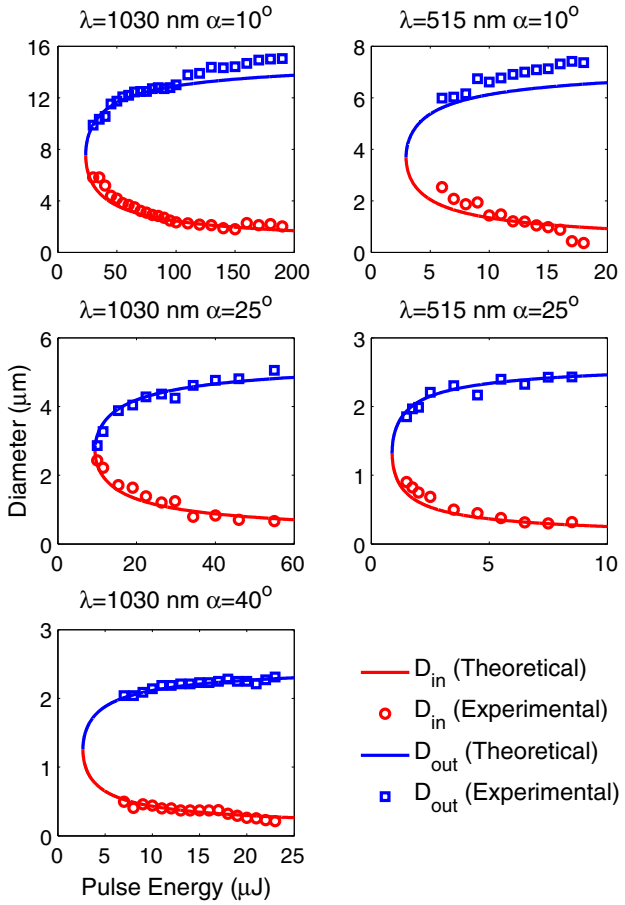

Fig. 4 Laser pulse energy versus inner/outer diameters of innermost ablation rings

particle can be made smaller by increasing pulse energy. In our experiments, we were able to obtain isolated disks with diameters as small as 200 nm. Further reduction of the disk size is limited by finite intensity in the vortex zone (cf. theoretical curves in Fig. 4) and minute variations in laser power and sample uniformity.

For pulse energies above $\sim$3 times the threshold, outer Bessel rings start to contribute to ablation. Very large ($\sim$10) number of concentric rings can be obtained, as shown in Fig. 3. We also observe that the multi-ring regime is very sensitive to the quality of Bessel beams. Irregularities at the beam profile are directly reflected on ablation patterns. The second harmonic generation process that we use to obtain shorter wavelength introduces fluctuations in the beam profile and causes detariorations on the sample as shown in Fig. 5, right part. This effect became prohibitive for the 40° axicon case, as the ablation feature sizes become comparable to irregularities.

Finally, in order to test the repeatability of the ablation experiments, we generated an array of 5 × 5 spots (in single-ring regime) over 200 μm × 200 μm area. We

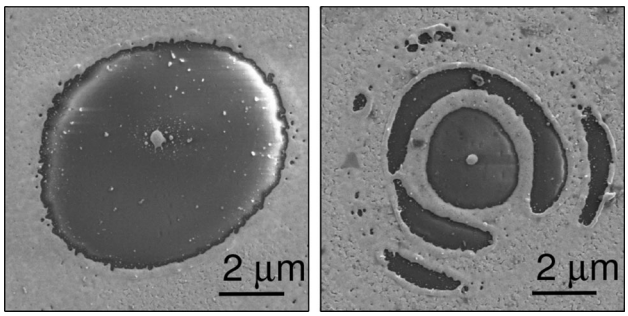

Fig. 5 *Left* SEM image of a gold nanodisk, fabricated with 515 nm wavelegnth and $\alpha = 10°$ axicon. *Right* irregular multi-ring pattern obtained with 515 nm wavelegnth and $\alpha = 25°$ axicon

observe that the ablation pattern is completely preserved throughout the entire region.

4 Conclusions

In conclusion, we demonstrated a detailed study of ablation behavior of Au thin films in single-pulse regime with fs laser pulses shaped to Bessel vortex beam profiles. The diffraction-free nature of Bessel beam provides convenience in sample positioning and significantly increases the repeatability of the experiments. Depending on the pulse fluence on sample surface, single or multiple ring structures can be fabricated. Ring dimensions can also be adjusted with fluence. This configuration could be of important advantages for fabrication of complex concentric structures or isolated nanodisks, as no mechanical scanning is necessary. Different ablation regimes we observe are open for applications such as generation of circular gratings [22], split-ring resonators [23] and nanoantennas [24, 25].

Acknowledgments This work was supported by Turkish Academy of Sciences (TUBA GEBIP). We also would like to thank Dr. Baris Yagci, Dr. Ozgur Birer from Koc University and Dr. Ali Kilic from Istanbul Technical University for SEM studies. R. Sahin also thanks TUBITAK for Ph.D. scholarship.

References

1. R.R. Gattass, E. Mazur, Nat. Photonics **2**(4), 219 (2008). doi:10.1038/nphoton.2008.47
2. S.I. Kudryashov, G. Mourou, A. Joglekar, J.F. Herbstman, A.J. Hunt, Appl. Phys. Lett. **91**(14), 141111 (2007). doi:10.1063/1.2790741
3. A. Joglekar, H. Liu, G. Spooner, E. Meyhfer, G. Mourou, A. Hunt, Appl. Phys. B **77**(1), 25 (2003). doi:10.1007/s00340-003-1246-z
4. A.P. Joglekar, H.h. Liu, E. Meyhfer, G. Mourou, A.J. Hunt, Proc. Nat. Acad. Sci. USA **101**(16), 5856 (2004). doi:10.1073/pnas.0307470101. http://www.pnas.org/content/101/16/5856.abstract
5. B. Yalizay, T. Ersoy, B. Soylu, S. Akturk, Appl. Phys. Lett. **100**(3), 031104 (2012). doi:10.1063/1.3678030

6. F. Courvoisier, P.A. Lacourt, M. Jacquot, M.K. Bhuyan, L. Furfaro, J.M. Dudley, Opt. Lett. **34**(20), 3163 (2009). doi:10.1364/OL.34.003163. http://ol.osa.org/abstract.cfm?URI=ol-34-20-3163
7. J. Durnin, J.H. Eberly, J.J. Miceli, Opt. Lett. **13**(2), 79 (1988). doi:10.1364/OL.13.000079. http://ol.osa.org/abstract.cfm?URI=ol-13-2-79
8. F. Courvoisier, J. Zhang, M. Bhuyan, M. Jacquot, J. Dudley, Appl. Phys. A **112**(1), 29 (2013). doi:10.1007/s00339-012-7201-2
9. R. Sahin, Y. Morova, E. Simsek, S. Akturk, Appl. Phys. Lett. **102**(19), 193106 (2013). doi:10.1063/1.4805358
10. R. Sahin, E. Simsek, S. Akturk, Appl. Phys. Lett. **104**(5), 053118 (2014). doi:10.1063/1.4864616
11. B. Wetzel, C. Xie, P.A. Lacourt, J.M. Dudley, F. Courvoisier, Appl. Phys. Lett. **103**(24), 241111 (2013). doi:10.1063/1.4846415
12. J. Nye, M. Berry, Proc. R. Soc. Lond. Ser. A Math. Phys. Eng. Sci. **336**(1605), 165 (1974). doi:10.1098/rspa.1974.0012
13. N.R. Heckenberg, R. McDuff, C.P. Smith, A.G. White, Opt. Lett. **17**(3), 221 (1992). doi:10.1364/OL.17.000221. http://ol.osa.org/abstract.cfm?URI=ol-17-3-221
14. M. Beijersbergen, L. Allen, H. van der Veen, J. Woerdman, Opt. Commun. **96**(13), 123 (1993). doi:10.1016/0030-4018(93)90535-D
15. S. Khonina, V. Kotlyar, M. Shinkaryev, V. Soifer, G. Uspleniev, J. Mod. Opt. **39**(5), 1147 (1992). doi:10.1080/09500349214551151
16. M. Beijersbergen, R. Coerwinkel, M. Kristensen, J. Woerdman, Opt. Commun. **112**(56), 321 (1994). doi:10.1016/0030-4018(94)90638-6
17. D. Grier, Nature **424**(6950), 810 (2003). doi:10.1038/nature01935
18. C. Hnatovsky, V.G. Shvedov, W. Krolikowski, A.V. Rode, Opt. Lett. **35**(20), 3417 (2010). doi:10.1364/OL.35.003417. http://ol.osa.org/abstract.cfm?URI=ol-35-20-3417
19. C. Hnatovsky, V.G. Shvedov, N. Shostka, A.V. Rode, W. Krolikowski, Opt. Lett. **37**(2), 226 (2012). doi:10.1364/OL.37.000226. http://ol.osa.org/abstract.cfm?URI=ol-37-2-226
20. J. Arlt, K. Dholakia, Opt. Commun. **177**(16), 297 (2000). doi:10.1016/S0030-4018(00)00572-1
21. J. Koch, F. Korte, T. Bauer, C. Fallnich, A. Ostendorf, B. Chichkov, Appl. Phys. A Mater. Sci. Process **81**(2), 325 (2005). doi:10.1007/s00339-005-3212-6
22. J.M. Steele, Z. Liu, Y. Wang, X. Zhang, Opt. Express **14**(12), 5664 (2006). doi:10.1364/OE.14.005664. http://www.opticsexpress.org/abstract.cfm?URI=oe-14-12-5664
23. M.C. Gwinner, E. Koroknay, L. Fu, P. Patoka, W. Kandulski, M. Giersig, H. Giessen, Small **5**(3), 400 (2009). doi:10.1002/smll.200800923
24. B. Lahiri, S.G. McMeekin, R.M. De La Rue, N.P. Johnson, Appl. Phys. Lett. **98**(15) (2011). doi:10.1063/1.3579537
25. H.M. Gong, L. Zhou, X.R. Su, S. Xioo, S.D. Liu, Q.Q. Wang, Adv. Funct. Mater. **19**(2), 298 (2009). doi:10.1002/adfm.200801151